

Upper Mantle Compressional Velocity Structure Beneath the Northwest Atlantic Ocean

LIAN-SHE ZHAO AND DON V. HELMBERGER

Seismological Laboratory, California Institute of Technology, Pasadena

A compressional velocity model for the northwest Atlantic Ocean is derived by modeling waveform and travel time data from long-period and short-period World-Wide Standard Seismograph Network and Canadian network station recordings. A 90-km-thick lid with a velocity of 8.1 km/s at the top gradually increasing to 8.3 km/s at the bottom is obtained by fitting the travel time data of first arrivals and waveform data of almost purely oceanic paths at distances of 8°-20°. Triplication P waveform data constrain the structure below the lid. A distinct but smooth low-velocity zone is located at a depth of 170 km. Combining these results with the shear wave structure derived by Grand and Helmberger (1984a) for the same region, we suggest an olivine-rich mineralogy in the upper 100 km and partial melting possibly extending as deep as 300 km based on low seismic velocities and high V_P/V_S .

INTRODUCTION

The dependence of the compressional and shear velocity structure on temperature and chemical composition continues to drive solid-state geophysical research. From published seismic velocity models, *Duffy and Anderson* [1989] and *Ita and Stixrude* [1992] derived possible mineralogies for the transition zones in the mantle. This field has become particularly interesting in light of the large lateral variations in seismic velocities revealed by recent global tomographic studies [e.g., *Anderson et al.*, 1992] and regional scale studies [*Zhao and Xie*, 1993].

Early global studies based on International Seismological Centre (ISC) travel times of P and S waves indicated major variations [e.g., *Clayton and Comer*, 1983]. More recent studies of differential travel times such as $SS-S$ have confirmed large lateral variability [Grand, 1987, also submitted manuscript, 1993; *Woodward and Masters*, 1991, 1992]. These studies show large-scale patterns of heterogeneity involving $SS-S$ time difference up to ± 12 s at teleseismic distances. These travel time differences are doubled at upper mantle triplication distances, and waveform data show distinct patterns in S and SS [Grand and Helmberger, 1984a,b]. The models displayed in Figure 1 are regionalized into shield (SNA), tectonic, and young ocean (TNA); the corresponding compressional velocity models are S25 [*LeFevre and Helmberger*, 1989] and GCA [*Walck*, 1984] respectively, and old ocean (ATL). Shield regions such as northeastern North America, SNA, display a prominent secondary phase at distances beyond 30° for S , and similarly, for SS beyond 60° [Grand and Helmberger, 1984b]. The ray paths responsible for the phase cross the relatively fast lid at low angles and bottom below the low-velocity zone. This phase, not seen in tectonic regions, can be modeled with a thick lid followed by a relatively smooth low-velocity zone extending to about 300 km. The shape of the velocity structure between 200 and 350 km is strongly controlled by the presence of this phase. A corresponding phase can, also, be observed in P and PP [*LeFevre and Helmberger*, 1989; *Schwartz and Lay*, 1993] in the SNA regionization (see S25

in Figure 1). This diagnostic phase is observed along the Atlantic coast for oceanic paths in S and SS as reported by *Grand and Helmberger* [1984a]. A shear velocity model appropriate for an old ocean, ATL, is developed in that study. It contains a prominent low-velocity zone which starts at a depth of 125 km and extends to a depth of 300 km. $SS-S$ times at teleseismic distances for this model are midway between TNA and SNA [*Grand and Helmberger*, 1984b] in agreement with the later study of *Woodward and Masters* [1991].

A corresponding P wave study for the ATL region has not been conducted, but a recent study by *Helmberger et al.* [1992] indicates that the P_n velocity drops 3 % crossing the New England suture zone from west to east, while the S_n velocities are nearly the same. This reduced P_n velocity should eliminate the extended triplication, as discussed above. The primary objective of this study is to establish this feature and derive the shallow P velocity structure down to 400 km appropriate for an old ocean, essentially the ATL regionization investigated by *Grand and Helmberger* [1984a].

DATA AND P_n TRAVEL TIMES

The data used in this study consist of the travel times obtained from short-period P waves and long-period P waveforms as recorded on the World-Wide Standard Seismograph Network (WWSSN) and Canadian Seismic Network (CSN) stations. Figure 2 displays the locations of the long-period stations and the events. Most of these events are associated with the tectonics of the Puerto Rico subduction zone (Table 1). The exceptions are event H, which is a large chemical explosion, and events L and I. The latter event, the Bermuda earthquake, produced most of the quality waveform data used in this study. This rare event occurred on an old fracture zone and was large enough to be recorded teleseismically. A detailed waveform modeling study by *Stewart and Helmberger* [1981] indicates a thrust mechanism located at a depth of 11 km. This orientation produced strong up going P wave energy, which coupled into the water-layer and generated a relatively strong coda.

The ray paths and travel times of the short-period data used in deriving the lid velocity structure are shown in Figure 3. The large stars show the events where we picked

Copyright 1993 by the American Geophysical Union.

Paper number 93JB00993.
0148-0227/93/93JB-00993\$05.00

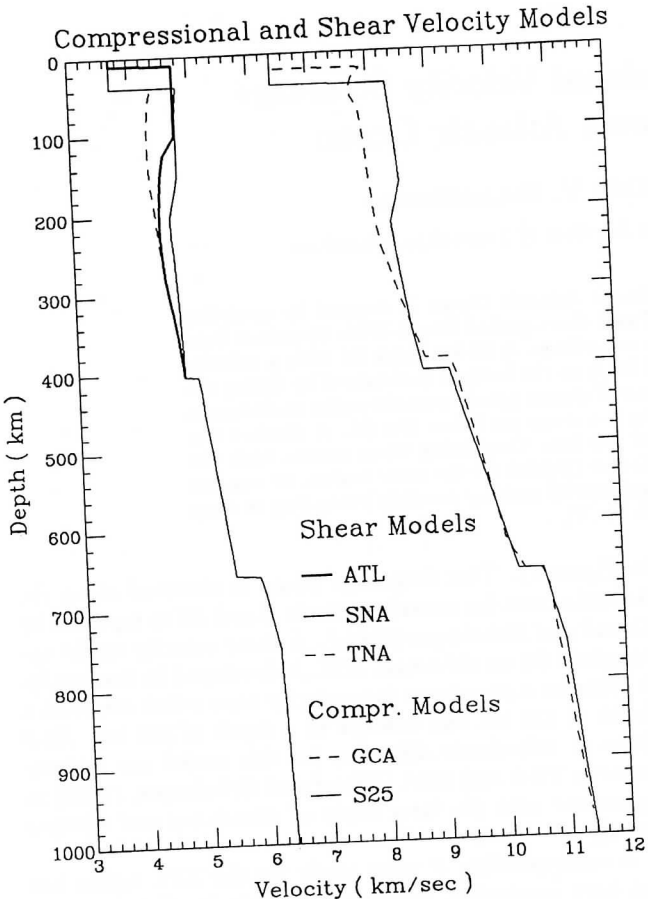


Fig. 1. Compressional and shear velocity models for different regionalizations. Models S25 [LeFevre and Helmberger, 1989] and GCA [Walck, 1984] are for shield, GCA [Walck, 1984] and TNA [Grand and Helmberger, 1984b] for tectonic and young ocean, and ATL [Grand and Helmberger, 1984a] for old ocean, respectively.

the travel times, and the small stars show the travel times taken from International Seismological Centre (ISC) bulletins. These times have been adjusted to place all events at the top of the mantle. These P wave travel time data were collected from more than 60 earthquakes. To avoid crustal complexities, we used the data from stations BEC, SJG, WES, and HAL only where the paths are almost purely oceanic. The distance range is 8° - 20° . We obtained the average velocity of 8.2 km/s in the lithosphere by least squares fitting these travel times (Figure 3b). The positive residuals are actually the vertical travel times of the P_n ray in the crust. In Figure 3b, the distance depending trend, the velocity of which is 8.2 km/s, was removed. The large standard error of 3.5 s for the data set plotted in Figure 3b apparently reflects the lateral variation in the structure, the errors in origin times and locations, and the difference between source structure and receiver structures. At present, it is difficult to resolve which effects are dominant without better control on source locations, but the average velocities are substantially lower than in shield structures.

MODELING RESULTS

The waveform modeling exercised here is similar to recent forward trial and error modeling efforts [see Zhao and Helmberger, 1991]. Two methods are employed: generalized

ray theory [Helmberger, 1983] and reflectivity [Mallik and Frazer, 1988]. The former is useful in searching the model space for the best model candidates; the latter yields complete seismograms for definitive testing. We will discuss models based on such waveform matching for the crust and lid followed by results for the upper mantle.

Crust and Lid Structure

We begin by testing the effectiveness of crustal models derived from oceanic refraction profiles in predicting the SJG observations of the Bermuda events. The best model given in Table 2 agrees well with previous studies [e.g., Christensen and Salisbury, 1975; Houtz and Ewing, 1975]. The shear velocities were obtained from the relationships given by Ludwig *et al.* [1970], except for the S_n velocity, which was adapted from Grand and Helmberger [1984a]. The results are displayed in Figure 4, in which the synthetics are appropriate for the displacement at the bottom of the fluid layer. This one-dimensional idealization is one treatment of the two-dimensional structure. Another will be discussed later.

This comparison is not particularly good for the onset of the P waves but shows some promise in the surface waveform fits. The SH waveform was addressed by Grand and Helmberger [1984a] and was one of the G phases used in the determination of the lid thickness. They found that to model the width of the first larger SH pulse required a lid thickness of about 90 km. It appears that the P onset and P_{nl} wave train comprising the first 50 s of the record contain information about the lid velocity structure. This feature is explored further in Figure 5. In subsequent sections it is convenient to treat the crust as a layer model, in which the vertical travel times across the crust are conserved, i.e., pP and sP times, etc. A crustal layer 10 km thick with a P velocity of 6.0 and S velocity of 3.6 km/s is a good approximation. The lid thickness is set at 90 km, to be compatible with SH wave study by Grand and Helmberger [1984a], and the velocity gradient is allowed to vary. This gradient zone is approximated by eight layers of homogeneous velocities as usually assumed in GRT modeling. Using the travel time constraints discussed in the previous section, we examined three cases. The velocity at the bottom of the zone is set at 8.3 km/s, which is roughly the upper bound based on the travel times and subjected to the constraint of the waveform modeling discussed later. The velocity at the top of the lithosphere is at 8.0, 8.1, and 8.2 km/s, and the resulting velocity gradient adjusts accordingly. Synthetics for these three cases generated with rays are displayed in Figure 5a, in which they are aligned in absolute time. Multiple bounces in the crustal waveguide are included, but multiple internal reflections in the lithosphere lid have been neglected. The model with a P_n velocity of 8.1 km/s fits best. This velocity agrees well with the average oceanic velocity of 8.13 [Raitt, 1963] and 8.1 km/s [Petterson *et al.*, 1974] for the top of the lid. Figure 5b displays the reflectivity results for the 8.1 km/s case. Note that the two solutions are quite compatible. The path from the Bermuda event to SJG is quite similar to paths from events occurring along the San Juan subduction zone to BEC (see Figure 2). The model discussed here agrees quite well with this set of waveform data, as discussed later.

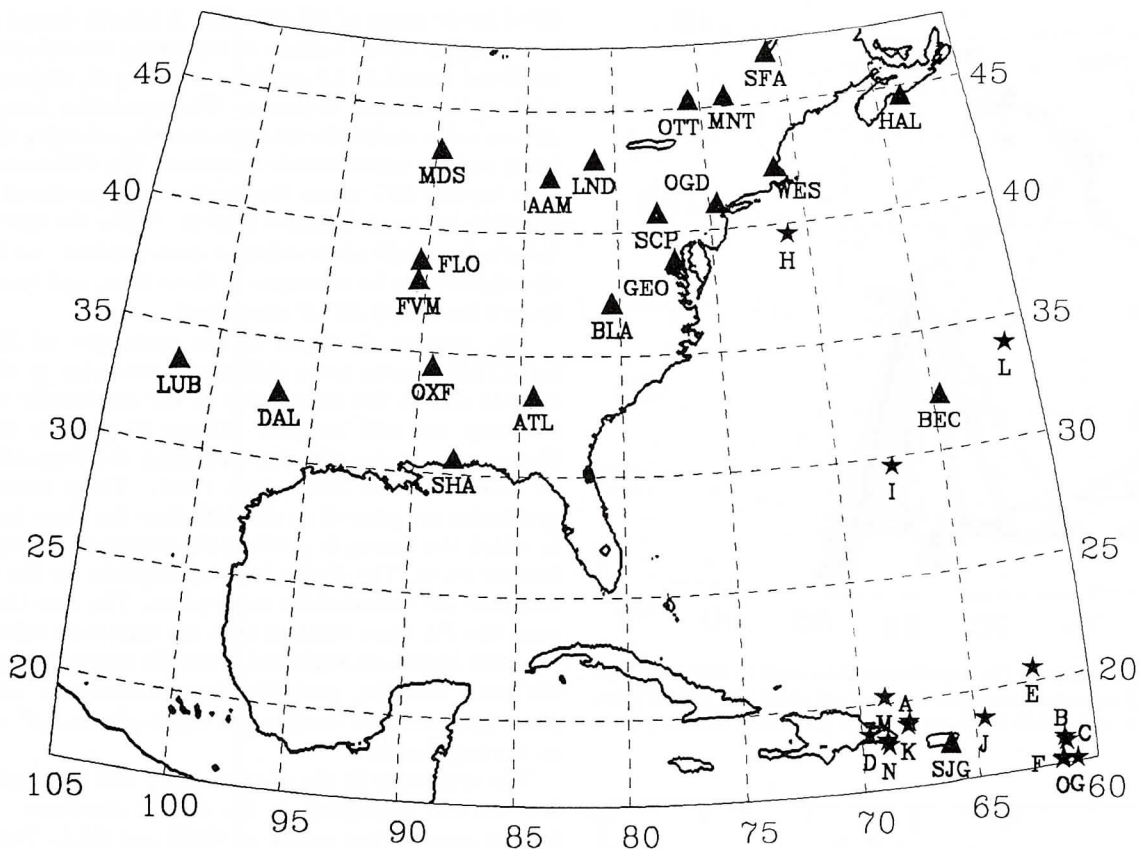


Fig. 2. Map showing area studied with the locations of events and stations used. Stars and triangles stand for the events and stations, respectively.

TABLE 1. Earthquakes

Event	Date	Time, UT	Lat. °N	Long. °W	Depth, km	<i>mb</i>
A	Nov. 3, 1966	1624:31.3	19.17	67.92	22	5.7
B	Dec. 24, 1967	2003:13.8	17.42	61.19	42	6.1
C	Dec. 24, 1967	2132:30.0	17.61	61.26	5	5.9
D	May 2, 1968	0529:37.7	18.80	69.69	75	5.6
E	Sept. 3, 1968	1537:00.3	20.58	62.30	10	5.6
F	May 15, 1969	2043:34.2	16.75	61.39	57	5.7
G	Dec. 1, 1969	2213:54.5	16.68	60.80	47	5.5
H	June 25, 1970	1608:54.8	39.62	71.07	0	5.0
I	March 24, 1978	0042:37.7	29.67	67.45	11	6.0
J	June 26, 1985	1710:01.9	18.91	64.60	48	5.6
K	July 21, 1985	1310:33.3	19.04	67.97	23	5.6
L	Dec. 9, 1987	0731:10.5	34.00	61.04	10	5.2
M	Sep. 27, 1980	0625:36.6	18.50	68.92	157	4.9
N	Sep. 14, 1981	1244:30.1	18.33	68.86	172	5.9
O	Jan. 30, 1982	0235:10.9	16.72	61.44	65	5.9

Upper Mantle Results

We begin with a short discussion of a useful one-dimensional idealization of the connection of an oceanic crust with a continental crust as shown in Figure 6. The model on the left is a two-dimensional diagram of a situation in which the events are located beneath the ocean with a thin crust and the stations are on land with a thick crust. We developed an analog model, shown on the right, which is one-dimensional but conserves travel times and can be used in generating accurate synthetics. The amplitude will be slightly modified due to the transmission differences along the upward path, as indicated by the dots. The source is situated at a greater depth in the analog model, and thus

the effects of *pP* and *sP* must be treated as part of the effective source function.

Figure 7 displays the synthetics generated from three oceanic models using this procedure for a simple impulsive *P* source. The three models are given in Figure 8, in which S25 is appropriate for a pure shield environment [LeFevre and Helmberger, 1989], ATLS is derived from Grand and Helmberger's [1984a] shear velocity model by assuming a smooth deep low-velocity zone and ATLP (Table 3) is the preferred model found in this study.

The triplication curves for these models are given in Figure 9, along with the short-period *P* wave travel times picked. Models are corrected to have a 15-km-thick crust. The travel times are calculated by assuming a source depth of 10 km, and the observed travel times are adjusted accordingly. The letters A, B, C, D, E, and F denote the branches. Branch AB is formed by the rays bottoming above the 400-km discontinuity, BC and CD branches are formed by the rays bottoming below the 400-km and above the 670-km discontinuities, and branches DE and EF are formed by the rays bottoming below the 670-km discontinuity. We will generally refer to branches by single letters, which will denote the two arrivals forming the cusp designated by the letter. With long-period data, the two geometric arrivals forming a branch usually cannot be distinguished. When there is possible confusion in the branch name, we will indicate a full designation. Note that the triplication curve of ATLP is distinctly different from those of ATLS and S25. Every branch of S25 is 3-5 s too fast. The B branch of ATLP ends at about 22°, but those of ATLS and S25 extend beyond 30°.

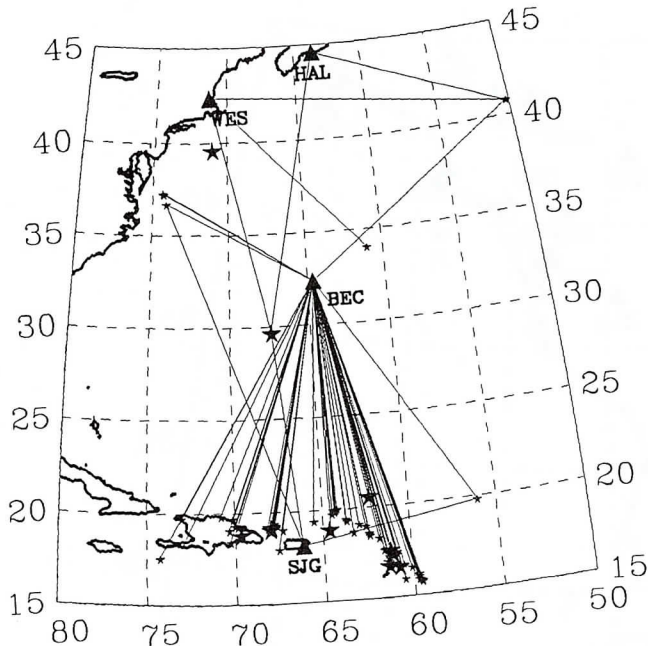


Fig. 3a. Ray paths of the travel time data used to determine the average lid velocity structure. Large stars show the events given in Figure 1 and Table 1. Note that the paths are almost purely oceanic.

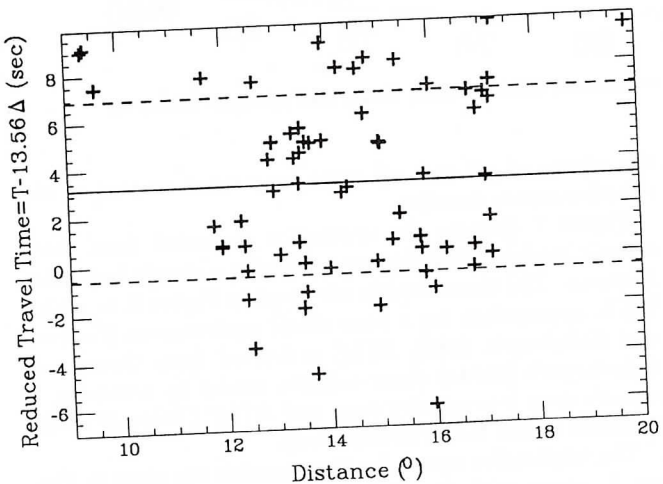


Fig. 3b. The travel time data for which paths are given in Fig. 3a. The solid line indicates an average velocity of 8.20 km/s. The pure time shift is 3.2 s, and standard error is 3.5 s.

TABLE 2. Crustal Model of Old Ocean

V_P , km/s	Q_α	V_S , km/s	Q_β	Density, Mg/m ³	Thickness, km
1.50	200	0.01	100	1.01	4.5
1.90	200	0.45	100	2.00	0.5
3.20	300	1.65	150	2.30	1.0
5.00	300	2.80	150	2.52	1.0
6.65	600	3.75	300	2.84	5.0
8.20	5000	4.75	2000	3.38	-

The synthetics for the models shown in Figure 8 contain only the down going rays and show the waveform complexity associated with the various upper mantle triplications (Figure 7). Synthetics associated with S25 display the simplest picture of conventional triplications with the AB simple branch produced by the velocity gradient in the thick lid branch followed by CD branch. These two phases are easily iden-

tified in the range of 12°-19°. The A branch decays rapidly in the ATLS model because of the strong low-velocity zone, while the model ATLP produces a strong P_n slightly ahead of A at the shorter distances. The synthetics from 19° to 25° are quite similar for all three models, reflecting the similarity in deep upper mantle structure. The differences reappear beyond 26°, where the shadow zone produced by the low-velocity zones becomes evident. While the extended B branch for shield observation is quite evident, we find little evidence for its existence in these data, and thus the B branch for model ATLP is subdued.

The features displayed in the synthetics of Figure 7 for ATLP become more difficult to recognize in observed records due to the complexity of the earthquake sources, but they can still be seen. Figure 10 presents the synthetic comparisons with the data from the Bermuda event as observed along the eastern coast. These records and synthetics are plotted in absolute time for those instances in which the timing is particularly important for this well-located event. The timing lines appropriate for the various branches are indicated for comparison. The rays that compose the PL wave train or that are internally reflected in the crust have been neglected, since the crustal waveguide is obviously complex, probably three-dimensional. However, these synthetics do contain the depth phases, pP and sP , as discussed earlier.

The synthetics fit the data at MNT and SHA quite well but are less convincing at the shorter distances. The A branch appears too strong at OGD and BLA. This could

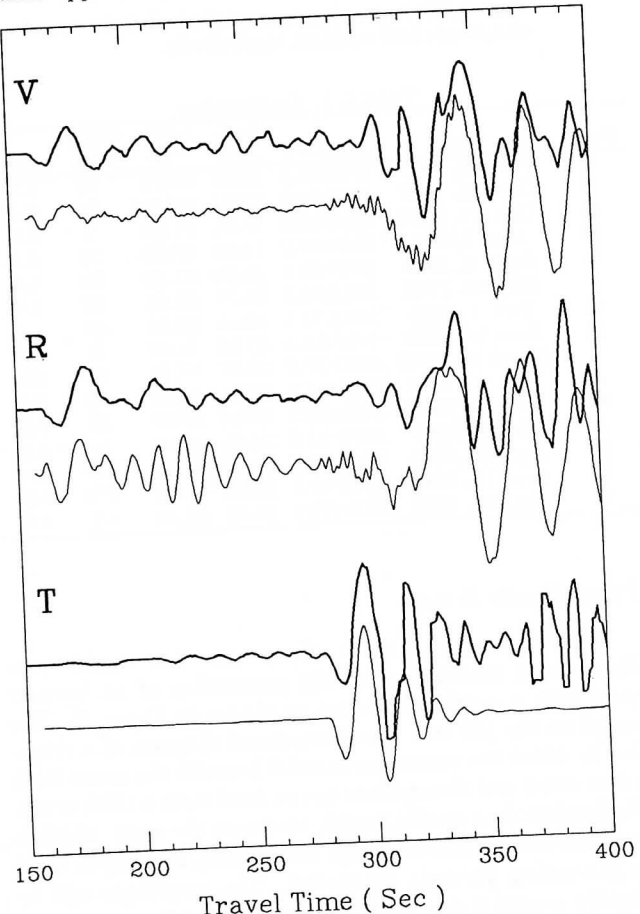


Fig. 4. Synthetic comparison of three components of whole records of a purely oceanic path, SJG to Bermuda earthquake.

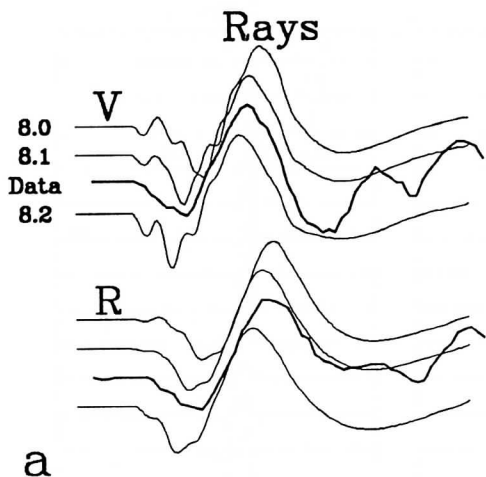


Fig. 5a. The beginning of 50 s of the SJG records and synthetics with different compressional velocities at the top of the lid. The synthetics include the P_{nl} waves and down going P waves.

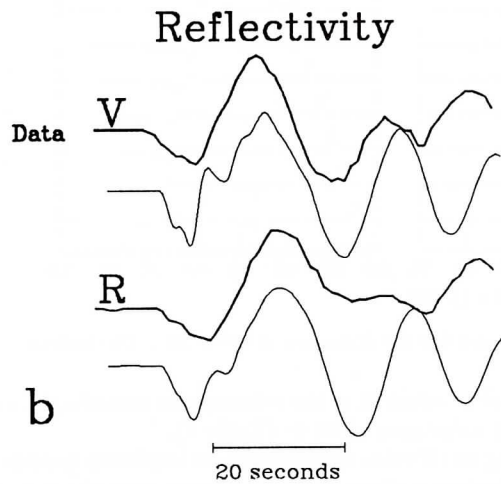


Fig. 5b. Comparison of the same SJG waveform with synthetics generated by reflectivity for the 8.1 km/s case.

be improved by decreasing the velocity gradient in the lid, which would enhance P_n as well as reduce the amplitude of branch A. On the other hand, a strong A branch is needed at ATL relative to P_n . However, the polarity of P_n changes in the synthetics, and thus the nearness to the radiation node becomes a problem. In any case, the relatively late arriving P_n and/or branch A in the data does not agree with the other two fast lid models which is the primary point of Figure 10.

Figure 11 presents the results of modeling some of the San Juan events recorded at the BEC station. Four of the simpler events were studied in detail, namely, event M, N, O, and J. We used the CMT source mechanisms as published in the ISC bulletins, namely (strike, dip, rake), given by M (279, 63, 55), N (263, 66, 92), O (334, 81, 100), and J (90, 29, 18). We assume the same source time function for all four events, described by a trapezoid (2, 2, 2). Since these events occurred in the mantle, their respective triplications appear at smaller ranges than do shallow events. The depth also strongly influences the P waves trapped in the crustal waveguide. To facilitate this situation, we have broken the synthetics into various contributions. The top row contains the reflectivity results from the upper portion of model discussed earlier, namely, the model down to a depth of 140 km. The next two rows display the ray responses where P_4 denotes the "400" discontinuity branch, P_L denotes the reflected energy from the low-velocity zone, and P_2 denotes the refracted energy from depth below 200 km (branch A). The summed synthetics fit the data quite well, and it appears that branch A is clearly seen, as in the seismic section from the Bermuda event. This further supports the ATLP model over the ATLS type of structure.

A comparison of synthetics for these three models against observations at larger ranges is given in Figure 12. The events used in Figure 12 have not been modeled telesismically. Thus we used P wave observations in the western United States as "effective source functions," denoted as events A, J, and K. The source function of event A is the DUG record, at a distance of 43.7° , that of event J is the seismogram recorded by station DUG at a distance of 46.4° ,

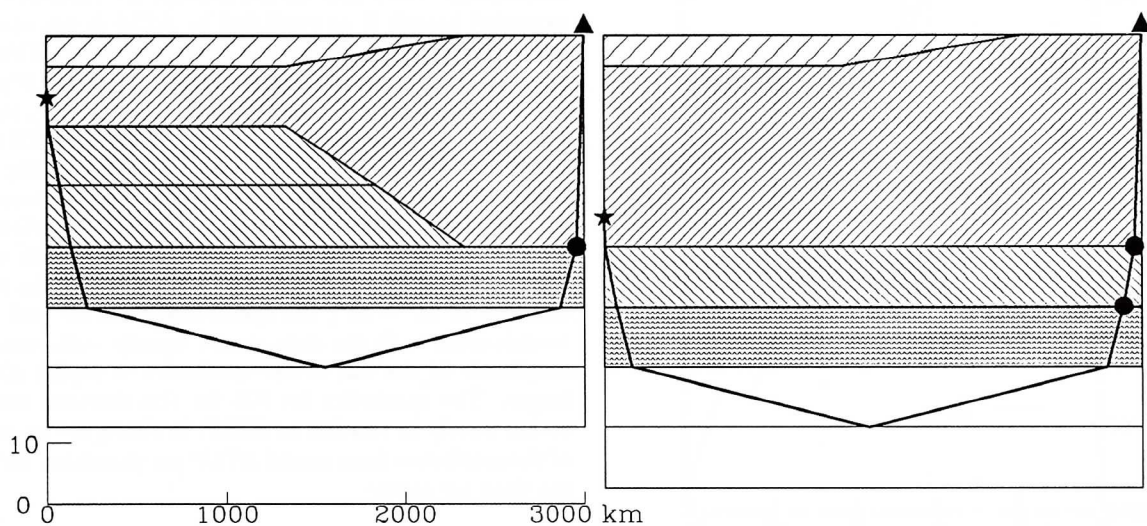


Fig. 6. (Left) Assumed to be the real model for oceanic-continental transition. (Right) The analog model constructed to preserve the travel times and amplitudes for down going rays. Stars are the sources; triangles are the receivers. The different patterns are assumed for various velocity layers.

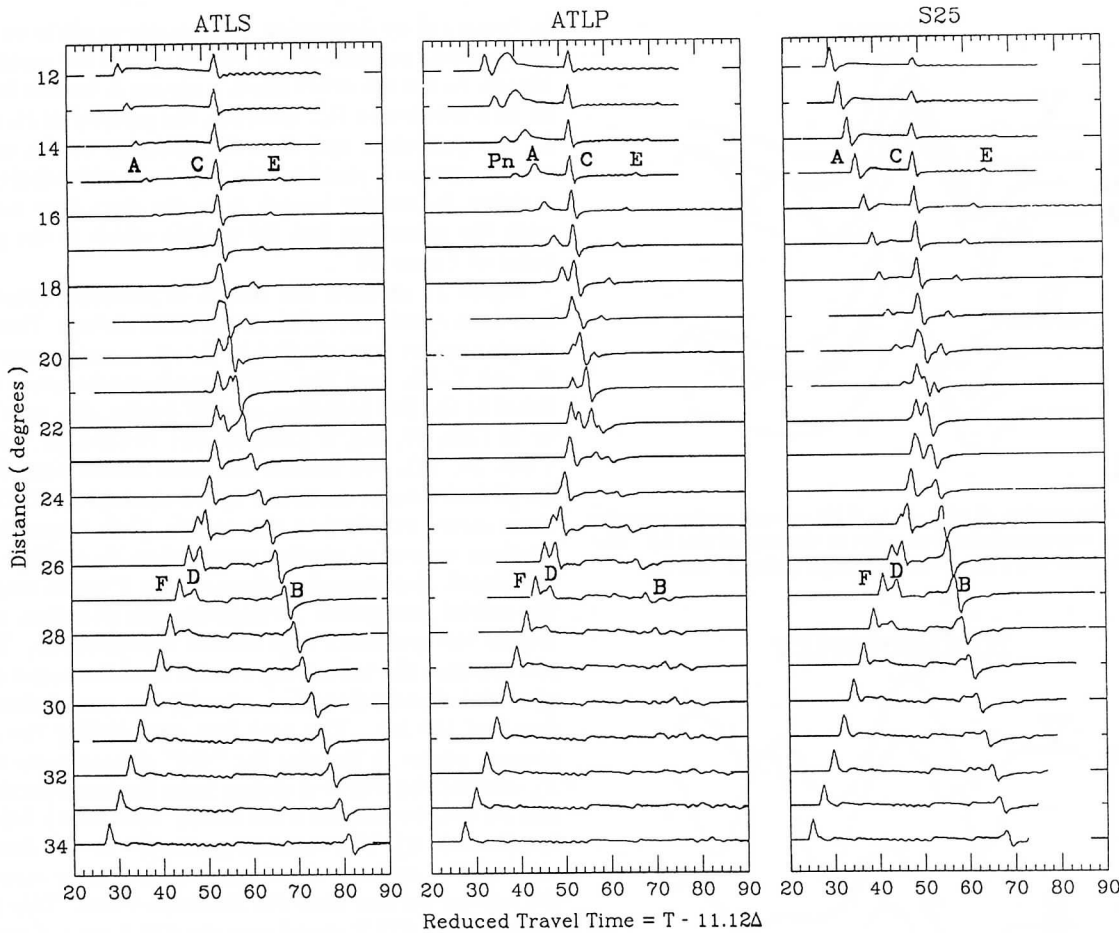


Fig. 7. Broadband waveforms predicted by models ATLP, ATLS, and S25 for distances of $12^\circ - 34^\circ$. The letters denote branches.

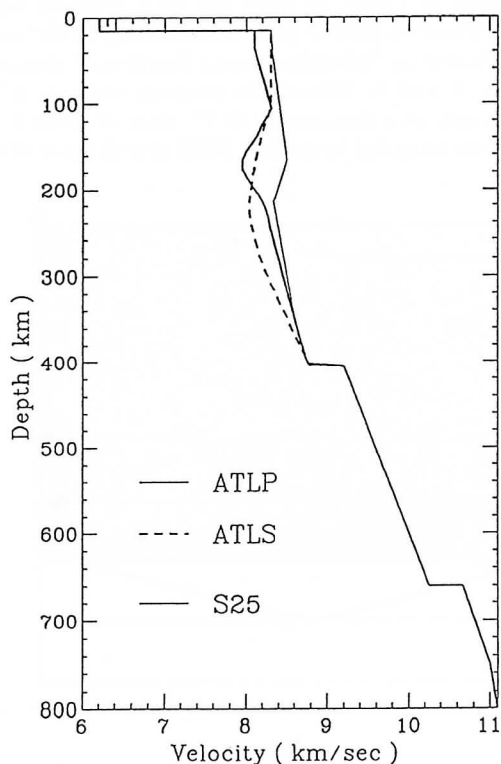


Fig. 8. The velocity model ATLP derived in this study, along with ATLS derived from shear velocity model, and S25 for Canadian Shield.

and that of event K is the seismogram recorded by station BKS at a distance of 50.5° (Table 1).

Using an effective source function implicitly assumes that the radiation pattern does not change over the ray parameter window encountered by the triplication. Since many events give consistent results, we believe this to be a valid assumption. Note that on the average the existence of the extended branch B as predicted by ATLS is not observed, while the waveform fit to ATLP is quite good. This is especially true at stations SHA (21.6°), BLA (22.9°), SHA (24.3°), FVM (27.2°) and FVM (29.5°). At 21.6° , the synthetics of all three models (ATLP, ATLS, and S25) show promising fits, except in the width of the first big pulse. This is due to all branches arriving almost at the same time for the models at this distance, as discussed earlier. The BLA recording of event J at a distance of 22.9° is fit well by the synthetics of ATLP and ATLS models. At the further distance of $24^\circ - 28^\circ$, the synthetics of ATLP and ATLS models seem to fit the data almost equally well, except the amplitude of the tail of the synthetics of model ATLS is larger. The synthetics for S25 for this distance range do rather poorly in relation to ATLP. In short, the overall fits of the synthetics from model ATLP are promising although the data are sparse.

DISCUSSION

This modeling study proved particularly difficult because of the lack of events and the problem of internal heterogeneity of the study area. Almost all stations are within the con-

TABLE 3. ATLP model

Depth, km	Velocity, km/sec
15	8.10
35	8.10
45	8.13
55	8.16
65	8.19
75	8.22
85	8.25
95	8.28
105	8.31
115	8.25
125	8.19
135	8.14
145	8.08
155	8.00
165	7.95
175	7.95
185	8.00
195	8.07
205	8.15
215	8.20
225	8.24
235	8.27
245	8.29
255	8.32
265	8.35
275	8.38
285	8.41
295	8.44
305	8.47
315	8.50
325	8.53
335	8.56
345	8.59
355	8.62
365	8.65
375	8.68
385	8.71
395	8.74
403	8.77
405	9.21
450	9.39
500	9.60
550	9.80
600	10.01
660	10.67
700	10.82
750	11.01
800	11.09
850	11.17
900	11.26
950	11.34

tinents, and all earthquakes are beneath the ocean. Since we corrected for the crustal thickness variations, the uncertainty is mostly confined to the lid and low-velocity zone. The compressional velocity, 8.1 km/s derived at the top of the mantle, beneath the northwestern Atlantic Ocean, is compatible with those beneath the Appalachian mountains [Helmberger *et al.*, 1992; Zhao and Helmberger, 1991] found in regional waveform modeling and those beneath eastern United States from deep seismic sounding studies [e.g., Braile, 1989]. This suggests that our one-dimensional analog model, connecting oceanic earthquakes to continental stations, is reasonable at least for the uppermost mantle down to a depth of order of 100 km.

The differential times and relative branch amplitudes of the waveform data at ranges $15^\circ - 35^\circ$ is diagnostic in modeling of the upper mantle velocity structure. The termination of branch D at ranges greater than 26° is due to a thick high-velocity lid followed by a deep low-velocity zone (ATLS and S25). That branches B and D are not observed

beyond 26° suggests that a lower-velocity lid is present. For example, the Tibetan Plateau data have all three branches B, D, and F coexisting with about the same amplitudes, while the model has no distinct low-velocity zone and the lid velocity is low [Zhao *et al.*, 1991]. As suggested by Zhao *et al.* [1991], a few high-quality triplication data can strongly constrain the upper mantle structure because of the resolving power of differential travel times between triplication branches.

The region sampled in this study covers lithosphere ages from 80 to 140 Ma and can be considered as "old ocean" in global regionalizations [e.g., Jordan, 1981]. This allows a comparison of the ATLP model with global averages of ($PP-P$) from Woodward and Masters [1991]. The results are given in Table 4 along with the comparisons in shields and tectonic provinces. The shear velocities are included as discussed previously by Woodward and Masters [1991]. If one interprets the TNA model as appropriate for young oceans as discussed by S. Grand [submitted manuscript, 1993], the comparisons become even better as discussed in the above studies.

Model ATLP displays a smooth low-velocity zone structure near 200 km that does not produce significant reflected energy which agrees with the recent result of Shearer [1991] and Revenaugh and Jordan [1991]. The jumps in the shear velocities at 405 and 660 are 4.5 and 7.2% in ATLP, in excellent agreement with the results of Revenaugh and Jordan [1991]. Thus there appears to be general agreement about the P and S velocities in the upper mantle, at least in the more stable regions.

Comparison of seismic velocities in mantle minerals, under mantle conditions, with seismic data is a first step toward constraining mantle chemistry. Figure 13 gives the comparison of the compressional and shear velocity structures derived for the northwest Atlantic Ocean, ATLP and ATL [Grand and Helmberger, 1984a]; Canadian Shield, S25

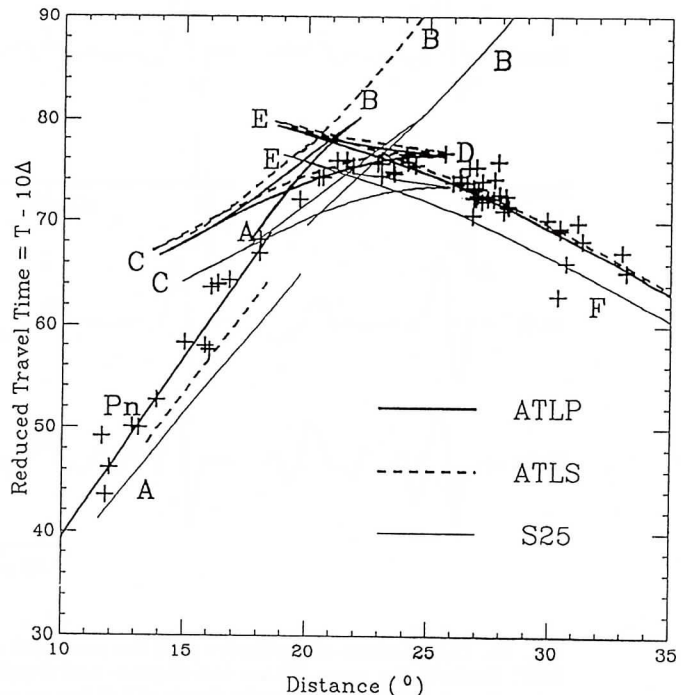


Fig. 9. Triplication curves predicted by models ATLP, ATLS, and S25, along with the travel time picks. The letters denote branches.

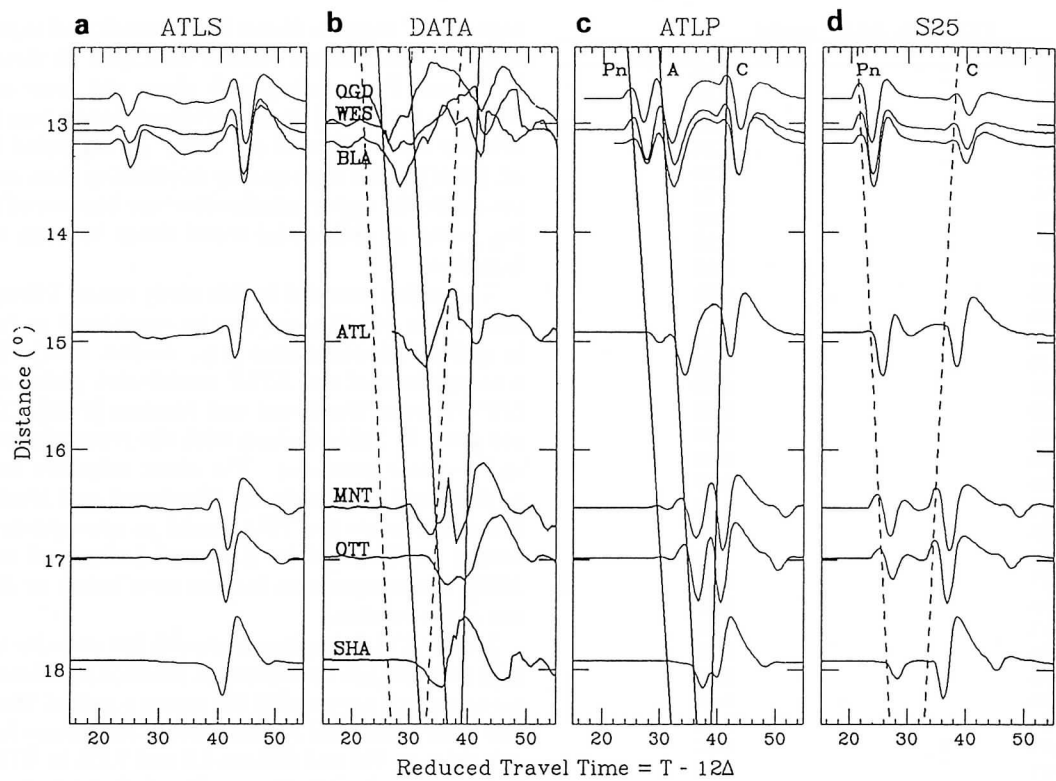


Fig. 10. (b) Bermuda earthquake data along with (a) synthetics of models ATLS, (c) ATLP, and (d) S25. The letters denote branches.

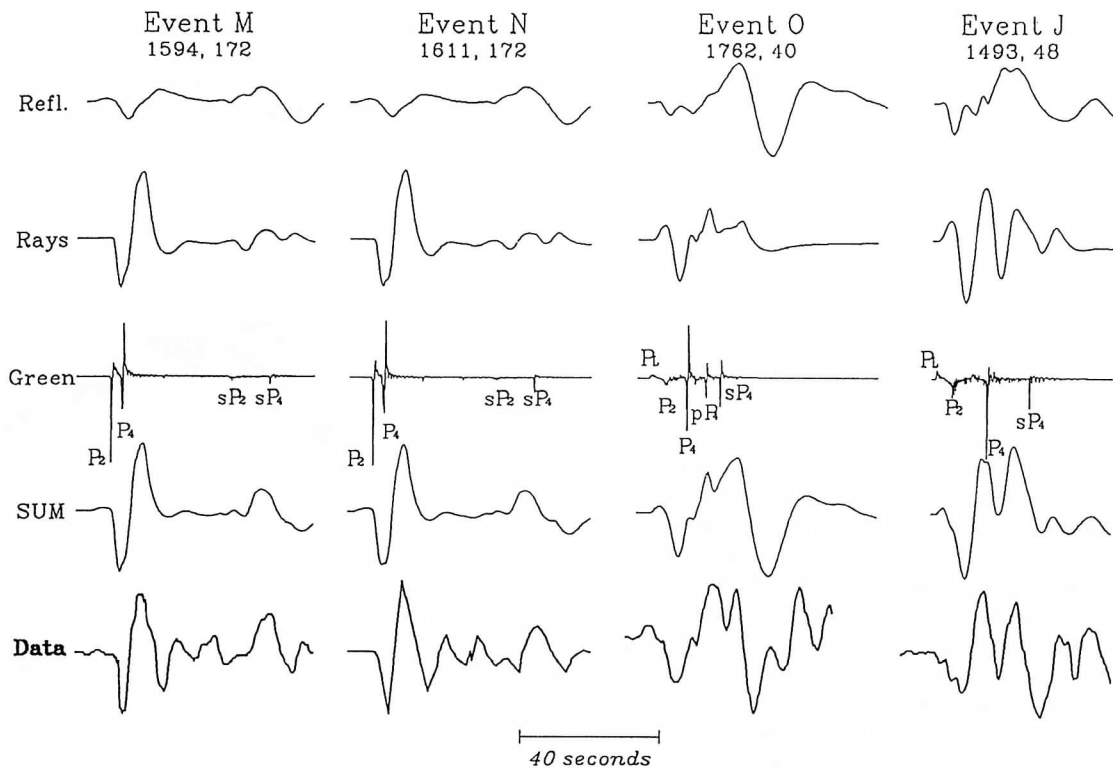


Fig. 11. Comparisons of synthetics with the pure path data from the San Juan Subduction Zone to the station BEC. Beneath the event ID are the distance and depth in kilometers. "Refl." means the reflectivity synthetics using the model ATLP up to the depth of 120 km or to source depth if the source is deeper. "Rays" means the synthetics of down going rays and their surface reflections, i.e., pP and sP and "Green" is the Green's function of "Rays." The sum of these two contributions is compared at the bottom.

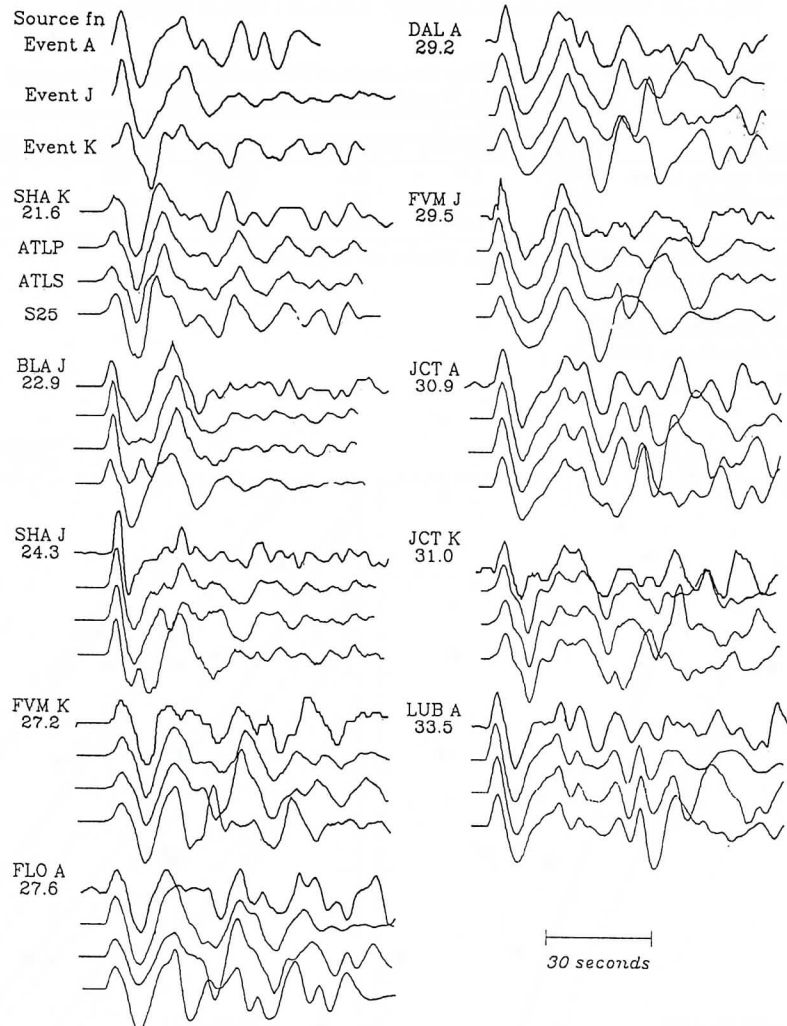


Fig. 12. Synthetic comparisons of models ATLP, ATLS, and S25 for distances of $21^\circ - 34^\circ$.

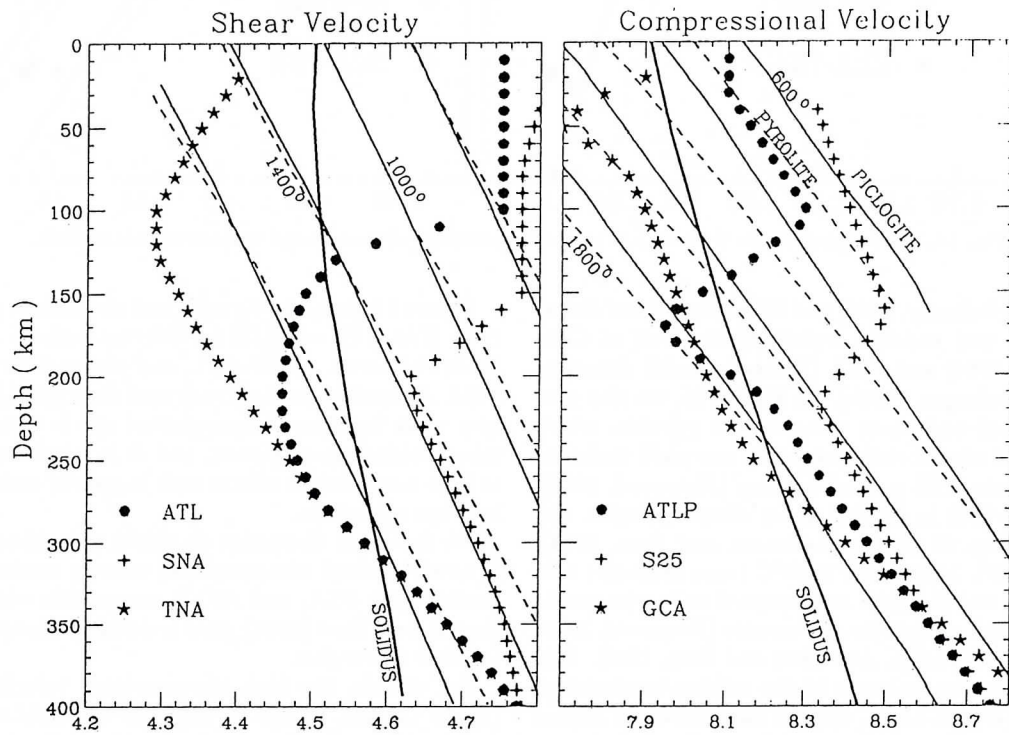


Fig. 13. Compressional and shear velocities for pyrolite and piclogite along various adiabats. The temperatures are for zero pressure. The solidus curves are from Wyllie [1984]. The portions of the adiabats below the solidus curves are in the partial melt field.

TABLE 4. Predicted Two-Way Travel Time Residuals of Different Models as Compared With the Observations of Woodward and Masters [1991]

Region	Model	$SS - S$		$PP - P$	
		Predicted	Observed	Model	Predicted
Tectonic and young ocean	TNA ^a	6.3	3.5	GCA ^b	1.9
Precambrian shield	SNA ^a	-5.7	-5.4	S25 ^c	-1.1
Old oceans	ATL ^d	0.2	0.2	ATLP ^e	0.0

Residuals are computed relative to PREM. Times are in seconds.

^a Grand and Helmberger[1984b];

^b Walck[1984];

^c LeFevre and Helmberger[1989];

^d Grand and Helmberger [1984a];

^eThis study.

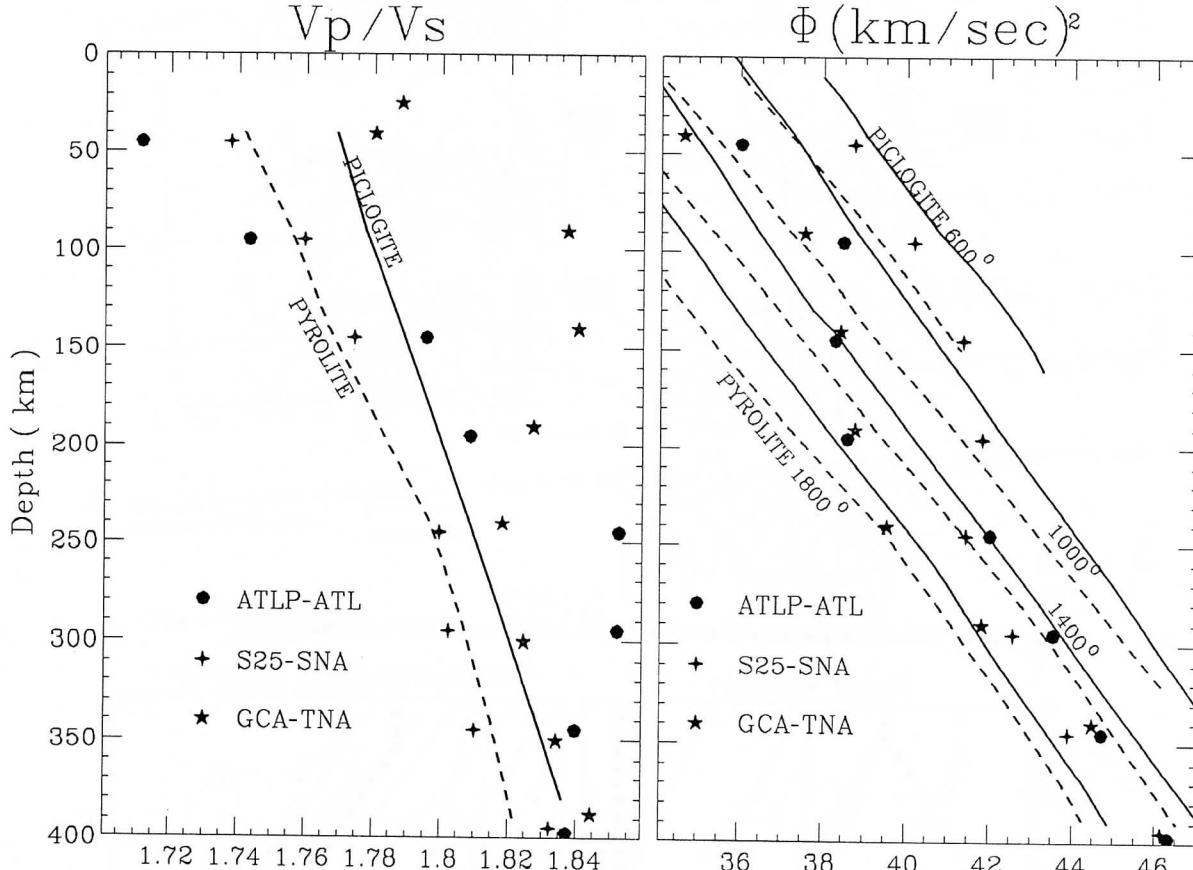


Fig. 14. Seismic parameter Φ and V_P/V_S for two petrological models and various seismic models.

[LeFevre and Helmberger, 1989] and SNA [Grand and Helmberger, 1984b]; and tectonic region, GCA [Gulf of California, Walck, 1984] and TNA [Tectonic North America; Grand and Helmberger, 1984b]. In Figure 13, we also give the compressional and shear velocities for pyrolite, which is a hypothetical olivine-rich rock which can yield tholeiitic magmas by about 25% partial melting [Ringwood, 1975], and piclogite, which is defined as an olivine eclogite, the high-pressure form of picrite [Anderson and Bass, 1984], along 600°, 1000°, 1400°, and 1800°C (zero pressure) adiabats. Pyrolite and piclogite are assumed to be the candidate mineralogical models for the mantle [Ringwood, 1975; Bass and Anderson, 1984; Anderson and Bass, 1986]. Figure 13 also shows an estimate of the solidus temperature of the mantle [Wyllie, 1984]. All the data shown in Figure 13 except the seismic velocity models are from Anderson and Bass [1984]. Ita and Stixrude [1992] listed the chemical compositions of pyrolite and piclogite.

Figure 14 gives V_P/V_S ratio and the seismic parameter Φ ($\Phi = K/\rho = V_P^2 - 4V_S^2/3$) for different regions: shields, S25-SNA; old ocean, ATLP-ATL; and rise and tectonic, GCA-TNA. According to Anderson and Bass [1984], V_P/V_S is a very weak function of temperature and is therefore a good mineralogical discriminant, and Φ is relatively insensitive to high temperature effects such as partial melting and dislocation relaxation.

We focus our discussion on shield and old ocean because of newly derived compressional velocity models S25, compatible with SNA, and ATLP, compatible with ATL. Anderson and Bass [1984] gave a detailed discussion for the tectonic rise region.

For shields, the high compressional velocity in the lid (upper 150 km, Figure 13) suggests very cold temperatures and/or high abundance of seismologically fast minerals, such as olivine or garnet. Low FeO content also increases seismic velocities. The rapid drop in velocity between 165

and 215 km requires a high temperature gradient or a decrease in the olivine content and an increase in the pyroxene content of the mantle [Anderson and Bass, 1984; Anderson, 1989]. The V_P/V_S ratio for the shield (Figure 14) favors an olivine-rich (pyrolite) mantle down to 400 km.

For the old ocean, the V_P of the lid (at upper 100 km) requires slightly warmer conditions than the shield model or has more olivine. From 100 to 170 km, there is a sharp velocity drop (Figure 13). It runs below the solidus at the depth of interval 140–200 km. Below 200 km, the V_P runs roughly parallel to the adiabats. The V_P/V_S ratio for the old ocean data (Figure 14) is very low in the upper 100 km. Increasing the olivine and orthopyroxene content or decreasing the FeO content of the old ocean lid relative to pyrolite would decrease V_P/V_S . Increasing orthopyroxene would decrease V_P . However, the V_P/V_S ratio for the old ocean data (Figure 14) is very high at the depth of 200–400 km, possibly the result of partial melting. Therefore the seismic properties of the old ocean lithosphere are best explained by an olivine-rich, possibly low FeO, peridotite with low temperatures and low temperature gradient [Anderson and Bass, 1984]. At 200–400 km depth, the mantle under old oceanic lithosphere appears to be partially melted, based on low seismic velocities and high V_P/V_S . For the shield region and upper 100 km of the old ocean, cold olivine-rich mineralogies are preferred.

CONCLUSIONS

We have modeled the long-period waveforms and short-period travel times of P waves to constrain the upper mantle compressional velocity model beneath the northwest Atlantic Ocean. The compressional velocity of the lithosphere is relatively low, 8.1 km/s at the top, and increases to possibly 8.3 km/s at the bottom of the lid. A low-velocity zone appears at depth of 170 km. The seismic data are consistent with an olivine-rich mineralogy in the upper 100 km and partial melting possibly extending as deep as 300 km.

Acknowledgments. Discussions with D. L. Anderson and P. J. Wyllie contributed greatly to this paper. We would also like to thank the two reviewers, P. Shearer and J. Revenaugh, for their excellent suggestions. We especially like to thank D. L. Anderson, who helped rewrite the section on mineralogical implications. This research was supported by National Science Foundation grant EAR-91-17781. Contribution 5172, Division of Geological and Planetary Sciences, California Institute of Technology, Pasadena, California.

REFERENCES

- Anderson, D. L., *Theory of the Earth*, Blackwell Scientific, Boston, Mass. 1989.
- Anderson, D. L., and J. D. Bass, Mineralogy and composition of the upper mantle, *Geophys. Res. Lett.*, 11, 637–640, 1984.
- Anderson, D. L., and J. D. Bass, Transition region of the Earth's upper mantle, *Nature*, 320, 321–328, 1986.
- Anderson, D. L., T. Tanimoto, and Y. S. Zhang, Plate tectonics and hotspots: The third dimension, *Science*, 256, 1645–1651, 1992.
- Bass, J. D., and D. L. Anderson, Composition of the upper mantle: Geophysical test of two petrological models, *Geophys. Res. Lett.*, 11, 237–240, 1984.
- Braile, L. W., Crustal structure of the continental interior, in *Geophysical Framework of the Continental United States*, edited by L. C. Pakiser and W. D. Mooney ed., Mem. Geol. Soc. Am. 1972, 285–315, 1989.
- Christensen, N. I., and M. H. Salisbury, Structure and constitution of the lower oceanic crust, *Rev. Geophys.*, 13, 57–86, 1975.
- Clayton, R. W., and R. P. Comer, A tomographic analysis of mantle heterogeneities from body wave travel times, *Eos Trans. AGU*, 64, 776, 1983.
- Duffy, T. S., and D. L. Anderson, Seismic velocities in mantle minerals and the mineralogy of the upper mantle, *J. Geophys. Res.*, 94, 1895–1912, 1989.
- Grand, S. P., Tomographic inversion for shear velocity beneath the North American plate, *J. Geophys. Res.*, 92, 14,065–14,090, 1987.
- Grand, S. P., and D. V. Helmberger, Upper mantle shear structure beneath the northwest Atlantic Ocean, *J. Geophys. Res.*, 89, 11,465–11,475, 1984a.
- Grand, S. P., and D. V. Helmberger, Upper mantle shear structure of North America, *Geophys. J. R. Astron. Soc.*, 76, 399–438, 1984b.
- Helmberger, D. V., Theory and application of synthetic seismograms, in *Earthquakes: Observation, Theory and Interpretation*, edited by H. Kanamori and E. Boshi, *Proc. Int. Sch. Phys. Enrico Fermi*, 85, 174–222, 1983.
- Helmberger, D. V., L. S. Zhao, D. Dreger, and V. LeFevre, Exploration of the lower lithosphere: Northeastern United States, *Phys. Earth Planet. Int.*, 70, 22–38, 1992.
- Houtz, R., and J. Ewing, Upper crustal structure as a function of plate age, *J. Geophys. Res.*, 81, 2490–2498, 1975.
- Ita, J., and L. Stixrude, Petrology, elasticity, and composition of the mantle transition zone, *J. Geophys. Res.*, 97, 6849–6866, 1992.
- Jordan, T. H., Global tectonic regionalization for seismological data analysis, *Bull. Seis. Soc. Am.*, 71, 1131–1141, 1981.
- LeFevre, L. V., and D. V. Helmberger, Upper mantle P velocity of the Canadian Shield, *J. Geophys. Res.*, 94, 17,749–17,765, 1989.
- Ludwig, W. J., J. E. Nafe, and C. L. Drake, Seismic refraction, in *The Sea*, Vol. 4, Part I, edited by A. E. Maxwell, pp. 53–84, Wiley-Interscience, New York, 1970.
- Mallick, S., and L. N. Frazer, Rapid computation of multi-offset vertical seismic profile synthetic seismograms for layered media, *Geophysics*, 55, 479–491, 1988.
- Peterson, J. J., P. J. Fox, and E. Schreiber, Newfoundland ophiolites and the geology of the oceanic layer, *Nature*, 247, 194–196, 1974.
- Raitt, R. W., The crustal rocks, in *The Sea*, Vol. 3, edited by M. N. Hill, pp. 85–102, Wiley-Interscience, New York, 1963.
- Revenaugh, J., and T. H. Jordan, Mantle layering from ScS reverberations, 3, The upper mantle, *J. Geophys. Res.*, 96, 19,781–19,810, 1991.
- Ringwood, A. E., *Composition and Petrology of the Earth's Mantle*, McGraw-Hill, New York, 1975.
- Schwartz, S. Y., and T. Lay, Complete PP waveform modeling for determining crust and upper mantle structure, *Geophys. J. Int.*, in press, 1993.
- Shearer, P. M., Constraints on upper mantle discontinuities from observations of long-period reflected and converted phases, *J. Geophys. Res.*, 96, 18,147–18,182, 1991.
- Stewart, G. S., and D. V. Helmberger, The Bermuda earthquake of March 24, 1978: A significant ocean intraplate event, *J. Geophys. Res.*, 86, 7027–7036, 1981.
- Walck, M. C., The P -wave upper mantle structure beneath an active spreading center: The Gulf of California, *Geophys. J. R. Astron. Soc.*, 76, 697–723, 1984.
- Woodward, R. L., and G. Masters, Global upper mantle structure from long-period differential travel times, *J. Geophys. Res.*, 96, 6351–6377, 1991.
- Woodward, R. L., and G. Masters, Upper mantle structure from long-period differential traveltimes and free oscillation data, *Geophys. J. Int.*, 109, 275–293, 1992.
- Wyllie, P. J., Constraints imposed by experimental petrology on possible and impossible magma sources and products, *Philos. Trans. R. Soc. London*, 310, 439–456, 1984.
- Zhao, L. S., and D. V. Helmberger, Broadband modeling along a shield path, Harvard recording of the Saguenay earthquake, *Geophys. J. Int.*, 105, 301–312, 1991.

- Zhao, L. S., and J. Xie, Lateral variations in compressional velocities beneath the Tibetan Plateau from P_n travel time tomography, *Geophys. J. Int.*, in press, 1993.
- Zhao, L. S., D. V. Helmberger, and Harkrider, D. G., Shear-velocity structure of the crust and upper mantle beneath Tibetan Plateau and Southeastern China, *Geophys. J. Int.*, 105, 713-730, 1991.

D. V. Helmberger and L.-S. Zhao, Seismological Laboratory, 252-21, California Institute of Technology, Pasadena, CA 91125.

(Received August 14, 1992;
revised March 8, 1993;
accepted April 12, 1993.)